Acta Pharmacologica Sinica

www.nature.com/aps

ARTICLE

Dual-omics reveals temporal differences in acute sympathetic stress-induced cardiac inflammation following α_1 and β-adrenergic receptors activation

Di Zhang[1], Ming-ming Zhao[2], Ji-min Wu[2], Rui Wang[2], Gang Xue[3], Yan-bo Xue[4], Ji-qi Shao[1], You-yi Zhang[2], Er-dan Dong[2], Zhi-yuan Li[1,3] and Han Xiao[2]

Sympathetic stress is prevalent in cardiovascular diseases. Sympathetic overactivation under strong acute stresses triggers acute cardiovascular events including myocardial infarction (MI), sudden cardiac death, and stress cardiomyopathy. α_1-ARs and β-ARs, two dominant subtypes of adrenergic receptors in the heart, play a significant role in the physiological and pathologic regulation of these processes. However, little is known about the functional similarities and differences between α_1- and β-ARs activated temporal responses in stress-induced cardiac pathology. In this work, we systematically compared the cardiac temporal genome-wide profiles of acute α_1-AR and β-AR activation in the mice model by integrating transcriptome and proteome. We found that α_1- and β-AR activations induced sustained and transient inflammatory gene expression, respectively. Particularly, the overactivation of α_1-AR but not β-AR led to neutrophil infiltration at one day, which was closely associated with the up-regulation of chemokines, activation of NF-κB pathway, and sustained inflammatory response. Furthermore, there are more metabolic disorders under α_1-AR overactivation compared with β-AR overactivation. These findings provide a new therapeutic strategy that, besides using β-blocker as soon as possible, blocking α_1-AR within one day should also be considered in the treatment of acute stress-associated cardiovascular diseases.

Keywords: adrenergic receptors; transcriptomics; proteomics; acute sympathetic stress; cardiac inflammation

Acta Pharmacologica Sinica (2023) 0:1–16; https://doi.org/10.1038/s41401-022-01048-5

INTRODUCTION

The sympathetic nervous system is activated to provoke the "fight or flight" reaction under acute stress conditions [1]. Sympathetic stress is prevalent in cardiovascular diseases. Under strong acute emotional or physical stress (i.e., anger, anxiety, distress, natural catastrophic disaster, car accident), overactivation of the sympathetic system can trigger acute cardiovascular events, including myocardial infarction (MI), sudden cardiac death, and stress cardiomyopathy [2]. In this case, massive endogenous catecholamines, norepinephrine, and epinephrine, were released to induce the pathologic response via adrenergic receptors (ARs) [3]. The dominant subtypes of ARs in the heart are α_1-ARs and β-ARs, both of which belong to the G protein-coupled receptor superfamily. Although the causality has been well established that acute stress can trigger cardiovascular events, little is known about the details of how sympathetic stress induces cardiac pathological changes over time [4]. Moreover, much less is known about whether and how α_1- and β-ARs differentially mediate the temporal responses.

Both receptor subtypes are essential for the physiological and pathologic regulation of the heart. α_1-ARs function in hypertrophy, positive inotropy, and ischemic preconditioning [5]. β-ARs constitute a major regulator of heart rate and contraction (positive inotropic and chronotropic effects) [6], which also lead to cardiac inflammation and fibrosis. Radioligand binding data in the heart suggest β-ARs account for nearly 90% of the total ARs density, and the other 10% AR are mainly α_1-ARs [7]. Accordingly, cardiac β-AR interventions have been extensively investigated, and β-blockers have been widely used to treat tachycardia, myocardial infarction, and heart failure [8]. By contrast, cardiac α_1-AR has been much less well studied, and α_1-AR blockers were primarily used to target vasoconstriction for treating hypertension [9]. However, recent studies suggested that both α_1-ARs and β-ARs should be considered dominant subtypes in the heart, as they are the only two subtypes presented in all individual ventricular myocytes [10]. At rest, a low dose of epinephrine only activates β-ARs. Under stress, both α_1-ARs and β-ARs can be activated [3, 11]. Therefore, α_1-ARs are likely to contribute to sympathetic stress-induced

[1]Center for Quantitative Biology, Academy for Advanced Interdisciplinary Studies, Peking University, Beijing 100871, China; [2]Department of Cardiology and Institute of Vascular Medicine, Peking University Third Hospital; NHC Key Laboratory of Cardiovascular Molecular Biology and Regulatory Peptides; Key Laboratory of Molecular Cardiovascular Science, Ministry of Education; Beijing Key Laboratory of Cardiovascular Receptors Research; Haihe Laboratory of Cell Ecosystem, Beijing 100191, China; [3]Peking-Tsinghua Center for Life Sciences, Academy for Advanced Interdisciplinary Studies, Peking University, Beijing 100871, China and [4]Department of Cardiovascular Medicine, First Affiliated Hospital of Xi'an Jiaotong University, Xi'an 710061, China
Correspondence: Er-dan Dong (donged@bjmu.edu.cn) or Zhi-yuan Li (zhiyuanli@pku.edu.cn) or Han Xiao (xiaohan@bjmu.edu.cn)
These authors contributed equally: Di Zhang, Ming-ming Zhao
These authors jointly supervised this work: Er-dan Dong, Zhi-yuan Li, Han Xiao

Received: 3 September 2022 Accepted: 28 December 2022
Published online: 03 February 2023

cardiac injuries in a manner distinct from that of β-ARs. Clarifying the functional similarities and differences between α_1- and β-ARs in stress-induced cardiac pathology is of great importance for the understanding and treatment of stress-associated cardiac issues.

Inflammation is an important pathological process in many sympathetic stress-associated cardiac diseases, such as arrhythmia [12], myocardial infarction [13], and heart failure [14]. In stress cardiomyopathy, stress-induced low-grade chronic inflammation subsequently evolves into long-term heart failure [15]. Our previous study demonstrated that acute sympathetic stress can initiate cardiac inflammation and dysfunction by activating the NLR family Pyrin domain containing 3 (NLRP3) inflammasome, which subsequently cleaves and activates interleukin-18 [16]. Both β-AR and α_1-AR activation can lead to this type of stress-induced cardiac inflammatory injury [16, 17]. At the genome scale, however, the role of α_1- and β-AR in acute sympathetic stress-induced inflammation has yet to be elucidated. In particular, the temporal responses in transcription and translation induced by α_1- and β-AR activation have not yet been explored in detail.

In this work, we systematically compared the genome-wide effects of acute β-AR and α_1-AR activation in the mice model by integrating transcriptome and proteome. In the present study, mice were treated with a single injection of selective β-AR and α_1-AR agonists, which allows for observing temporal profiles in the heart following treatment. Combining exploratory data analysis with biochemical validation, we traced the differential responses induced by α_1-AR and β-AR in their upstream causes and downstream consequences by dual-omics data integration. We found that α_1-AR activation mediated additional signaling and effects than β-AR, which provides novel therapeutic strategies for sympathetic stress-induced cardiac injury.

MATERIALS AND METHODS

Animals

All animal experiments were approved by Peking University Institutional Review Board Animal Welfare Committee (LA2021013) and conformed to the guidelines for animal experiments of Peking University Health Science Center. The 12-week-old male C57BL/6N mice were bought from Vital River Laboratory Animal Technology Company (Beijing, China) and housed in a specific pathogen-free environment in the Animal Department of Peking University Health Science Center. Mice were randomly allocated into different groups and subcutaneously injected with a single dose of isoprenaline (ISO, 5 mg/kg) or phenylephrine (PE, 10 mg/kg). The dosage was chosen according to our previous studies [16, 17]. In the experiments with NF-κB inhibitor, mice were pretreated with Bay11-7082 (5 mg/kg body weight) intraperitoneally in a final volume of 100 μl of saline. Then mice were subcutaneously injected with a single dose of phenylephrine (PE, 10 mg/kg). After 1 h, 1 day, or 3 days, mice were euthanatized following anesthetization with an overdose of pentobarbital. The heart tissue was collected for further determination. RNA-Seq and protein mass spectrometry were performed using the heart tissue from the same heart.

Reagents and antibodies

ISO (Sigma-aldrich, St. Louis, MO, USA; Catalog I5627), PE (Sigma-aldrich; Catalog PHR1017), NF-κB inhibitor Bay11-7082 (MedChemExpress, China, Catalog HY-13453), dihydroethidium (DHE; Thermo scientific, USA, Catalog D11347), CD68 antibody (Servicebio, Wuhan, China; Catalog GB113109), Ly6G antibody (Servicebio, Catalog GB11229), P65 antibody (Cell Signaling Technology, USA; Catalog 4764), phosphorylated P65 antibody (Cell Signaling Technology USA; Catalog 3033), pyruvate dehydrogenase (PDH; Cell Signaling Technology USA; Catalog 3205S), isocitrate dehydrogenase 2(IDH2; Cell Signaling Technology USA; Catalog 56439S) COX IV (Cell Signaling Technology USA; Catalog 11967S), integrin α5 (ITGA5; Cell Signaling Technology USA; Catalog 4705S), S100A9 (Cell Signaling Technology USA; Catalog 73425S), NDUFA8 (Solarbio China; Catalog K107454P), heat shock protein β1 (HSPB1; Solarbio China; Catalog K000488P), glyceraldehyde-3-phosphate dehydrogenase (GAPDH; Cell Signaling Technology; Catalog 97166).

RNA extraction and library construction

A total amount of 1 μg RNA was used as input material for the RNA sample preparations. mRNA was purified from total RNA by using poly-T oligo-attached magnetic beads. Fragmentation was carried out using divalent cations under elevated temperature in First Strand Synthesis Reaction Buffer(5X). First-strand cDNA was synthesized using random hexamer primer and M-MuLV Reverse Transcriptase, then RNaseH was used to degrade the RNA. Second-strand cDNA synthesis was subsequently performed using dNTP with DNA Polymerase I system. After adenylation of 3′ ends of DNA fragments, the adapter with hairpin loop structure was ligated for hybridization. To select cDNA fragments of preferentially 250–300 bp in length, the library fragments were purified with the AMPure XP system (Beckman Coulter, Beverly, USA). After PCR amplification, the PCR product was purified by AMPure XP beads, and the library was finally obtained. To ensure the quality of the library, the library was initially quantified by Qubit2.0 Fluorometer, then diluted to 1.5 ng/μl, and the insert size of the library is detected by Agilent 2100 bioanalyzer. After insert size meets the expectation, qRT-PCR is used to accurately quantify the effective concentration of the library (the effective concentration of the library is higher than that of 2 nM) to ensure the quality of the library.

Deep sequencing and mapping

Deep sequencing was done by Illumina NovaSeq 6000 with settings of pair-end and 150 bp-long read length. Data manipulation included removing reads containing adapter, reads containing poly-N, and low-quality reads from raw data. Then the clean reads were mapped to the mouse reference genome GRCm38.p6 from the National Center for Biotechnology Information (NCBI) database using Hissat2 v2.0.5 [18].

Analysis of deep-sequencing data

Genes with zero counts in all samples were filtered out, leaving 24,188 genes under ISO treatment and 23,526 genes under PE treatment. The mRNA levels were normalized to gene length and total counts as transcripts per million (TPM). Then the principal component analysis was performed with Matlab. Differential expression analysis between conditions was performed using the DESeq2 R package [19]. We screened for differentially expressed genes with abs(log2(mRNA fold change)) >1 and P value was adjusted < 0.05.

Next, functional enrichment analysis was carried out using enrichGO in R package clusterProfiler [20]. In addition, genome-wide annotation org.Mm.eg.db for mouse was used. KEGG pathway enrichment analysis was carried out using enrichKEGG in R package clusterProfiler [20]. The enrichment results were filtered with an adjusted P value < 0.05. The visualization of pathway gene expression was performed using R package Pathview. And pathway information was obtained from the KEGG database. All other data analysis was performed with R and Matlab.

Protein extraction and trypsin treatment

The sample was ground individually in liquid nitrogen and lysed with lysis buffer containing 100 mM NH_4HCO_3(pH 8), 6 M urea, and 0.2% SDS, followed by 5 min of ultrasonication on ice. The lysate was centrifuged at 12,000 g for 15 min at 4 °C and the supernatant was transferred to a clean tube. Extracts from each sample were reduced with 10 mM DTT for 1 h at 56 °C and subsequently

alkylated with sufficient iodoacetamide for 1 h at room temperature in the dark. Then samples were completely mixed with four times volume of precooled acetone by vortexing and incubated at −20 °C for at least 2 h. Samples were then centrifuged and the precipitation was collected. After washing twice with cold acetone, the pellet was dissolved by dissolution buffer, which contained 0.1 M triethylammonium bicarbonate (TEAB, pH 8.5) and 6 M urea.

Then 120 μg of each protein sample was taken and the volume was made up to 100 μL with lysis buffer. 3 μL of 1 μg/μL trypsin and 500 μL of 50 mM TEAB buffer were added. The sample was mixed and digested at 37 °C overnight. An equal volume of 1% formic acid was mixed with the digested sample and centrifuged at 12000 ×*g* for 5 min at room temperature. The supernatant was slowly loaded to the C18 desalting column, washed with 1 mL of washing solution (0.1% formic acid, 4% acetonitrile) 3 times, and eluted twice by 0.4 mL of elution buffer (0.1% formic acid, 75% acetonitrile). Then the eluents were combined. All samples were mixed with equal volume and lyophilized, and the remaining eluent of each sample was lyophilized respectively.

DDA spectrum library construction

For transition library construction, shotgun proteomics analyses were performed using an EASY-nLC™ 1200 UHPLC system (Thermo Fisher) coupled with a Q Exactive HF-X mass spectrometer (Thermo Fisher) operating in the data-dependent acquisition (DDA) mode. The separated peptides were analyzed by Q Exactive HF-X mass spectrometer (Thermo Fisher), with ion source of Nanospray Flex™ (ESI), spray voltage of 2.5 kV, and ion transport capillary temperature of 320 °C. Full scan ranged from m/z 350 to 1500 with resolution of 60,000 (at *m/z* 200), an automatic gain control (AGC) target value was 3×10^6 and a maximum ion injection time was 20 ms. The top 40 precursors of the highest abundant in the full scan were selected and fragmented by higher-energy collisional dissociation (HCD) and analyzed in MS/MS, where resolution was 15,000 (at *m/z* 200), the AGC target value was 1×10^5, the maximum ion injection time was 45 ms, normalized collision energy of 27%, and intensity threshold of 2.2×10^4, and the dynamic exclusion parameter of 40 s. The raw data of MS detection was used to construct the DDA spectrum library.

LC-MS/MS analysis for DIA mode

The lyophilized powder of each sample was dissolved in 12 μL of A solution (0.1% FA in H_2O), centrifuged at 15,000 rpm for 20 min at 4 °C, and each supernatant was added to 0.4 μL of the standard peptide. Then 1 μg of the sample was injected into the EASY-nLC™ 1200 UHPLC system (Thermo Fisher) coupled with an Orbitrap Q Exactive HF-X mass spectrometer (Thermo Fisher) operating in the data-independent acquisition (DIA) mode with spray voltage of 2.5 kV, Nanospray Flex™ (ESI) and capillary temperature of 320 °C. For DIA acquisition, the *m/z* range covered from 350 to 1500. MS1 resolution was set to 60,000 (at *m/z* 200). The full scan AGC target value was 3×10^6. The maximum ion injection time was 50 ms. Then peptides were fragmented by HCD in MS2, in which resolution was set to 30,000 (at 200 *m/z*), AGC target value was 1×10^6, normalized collision energy of 27%.

Protein quantitation and data analysis

DDA and DIA data were analyzed using Proteome Discoverer 2.2 (PD 2.2, Thermo) platform, Biognosys Spectronaut version 9.0, and R statistical framework. DDA MS raw files were analyzed by PD software (version 2.2) and peak lists were searched against the protein database. MS1-based label-free quantification (LFQ) was done using the maxLFQ algorithm [21]. MS2-based-label-free quantification was carried out by analyzing DIA raw data using Biognosys Spectronaut (version 9.0) software. Data analysis was carried out as described in Bruder et al. with minor modifications [22].

After protein quantitation, proteins with zero expression in all samples were filtered out, leaving 2036 proteins under ISO treatment and 3255 proteins under PE treatment. Differential expression analysis of protein MS between conditions was performed using the DESeq2 R package [19]. We screened for differentially expressed genes with abs(protein MS fold change) >1.2 and adjusted *P* value < 0.05. Subsequent functional enrichment analysis was consistent with that in RNA-Seq.

Quantitative real-time PCR

Total RNA was extracted from heart tissue using TRIzol reagent (Invitrogen, Carlsbad, CA, USA Catalog 15596026). The RNA samples were reverse transcripted to cDNA, and the expression of genes was determined by real-time PCR with the Applied Biosystems QuantStudio 3 System. The relative expression of targeted genes was calculated as a ratio to that of GAPDH. The primers were as follows (5'-3'), Cxcr2 forward ATGCCCTCTATTCTGCCAGAT and reverse GTGCTCCGGTTGTATAAGATGAC, Rgs2 forward GAGAAAATG AAGCGGACACTCT and reverse GCAGCCAGCCCATATTTACTG, Ccrl2 forward GCCCCGGACGATGAATATGAT and reverse CACCAAGATAAA-CACCGCCAG, Tnf forward CCCTCACACTCAGATCATCTTCT and reverse GCTACGACGTGGGCTACAG, Il6 forward TAGTCCTTCCTACCCC AATTTCC and reverse TTGGTCCTTAGCCACTCCTTC, Il18 forward GAC TCTTGCGTCAACTTCAAGG and reverse CAGGCTGTCTTTTGTCAACGA, Il1b forward GCAACTGTTCCTGAACTCAACT and reverse ATCTTTTGGG GTCCGTCAACT, Gapdh forward AGGTCGGTGTGAACGGATTTG and reverse TGTAGACCATGTAGTTGAGGTCA.

Immunohistochemistry

The heart tissue was fixed with 4% paraformaldehyde and embedded in paraffin. The tissue was cut into serial sections and incubated with antibodies against the marker of immune cells. Macrophages and neutrophils were stained with antibodies against CD68 and Ly6G, respectively. Tissue sections were imaged with the NanoZoomer-SQ Digital slide scanner (Hamamatsu, Japan). The size of the positive area was calculated with the ImageJ software.

ROS measurement

Cardiac ROS levels were determined by DHE staining. Briefly, a freshly harvested heart was embedded with optimal cutting temperature compound within 10 min and cut into slices within 2 h, then incubated for 30 min at 37 °C with DHE (5 μM). The slides were covered using a mounting medium with DAPI. The slides were examined using a laser confocal microscope with an excitation maximum of 535 nm and an emission maximum of 610 nm.

ATP measurement

ATP level was determined using ATP Determination Kit (Thermo Scientific, USA, Catalog A22066). Fresh cardiac tissue was homogenized in a mixture containing radioimmunoprecipitation assay buffer and the protein content was determined using a Bradford protein assay kit. ATP levels were measured according to the manufacturer's instructions. Finally, the ATP level was normalized by the protein concentration.

Western blotting

Western blotting experiments were performed according to the guide from Tie et al. [23]. The lysate of cardiac tissue was subjected to SDS-PAGE electrophoresis and blotted on nitrocellulose membranes. The membranes were incubated with first antibodies overnight at 4 °C, and then with corresponding second antibodies. The blots were visualized with Thermo Scientific Pierce ECL detection reagent and imaged with GeneGnome chemiluminescence imaging system (Syngene, Frederick, MD, USA). The relative expression is calculated according to the gray value of blots with the ImageJ software.

Statistical analysis

Results were presented as mean ±SEM, and sample sizes were listed in figure legends. The statistics analysis was performed using one-way ANOVA with an LSD post hoc test. $P < 0.05$ was considered statistically significant.

Protein-protein association analysis

Protein-protein association analysis was performed using STING [24]. All types of interactions were included in this study.

RESULTS

Transcription profiles revealed differences between β-AR and α_1-AR activation

To obtain temporal profiles of the inflammatory responses, we separated mouse heart tissues at time points of 1 h and 1 day after β-AR agonist (Isoproterenol, ISO) and α_1-AR agonist (phenylephrine, PE) treatment. Then RNA and protein were extracted for RNA-Seq and protein mass spectrometry, respectively (Fig. 1a). After filtering out low expression genes for RNA-Seq, 24,188 and 23,526 genes were reserved for subsequent analysis of ISO and PE treatments, respectively.

To gain a global understanding of the distinctions between β-AR and α_1-AR activation, we analyzed the correlation of gene expressions from RNA-Seq between experimental conditions and replicates. For ISO treatment, the RNA-Seq data showed high Pearson correlation coefficients between replicates, indicating reliable measurements (Fig. 1b). The gene expression profile changed drastically 1 h after ISO treatment but reverted to be similar to the control group on day 1. This pulse-like dynamic was also evident in the principal component analysis of the gene expression profile (Fig. 1c). For PE treatment, expression profiles between replicates were also highly correlated (Fig. 1d), while their temporal dynamics were consistently distinct from those of ISO treatment. Although there was a considerable difference between the 1-h samples and the control group, the disparity between the 1-day samples and the control was even more significant (Fig. 1d,e). These findings suggested that the dynamics of the expression profiles caused by ISO and PE are markedly different. β-AR agonist ISO induces more transient changes that cease within a day, whereas α_1-AR agonist PE induces more long-lasting effects.

We further searched for differentially expressed genes after each type of treatment. As illustrated by the volcano diagrams, there were more differentially expressed genes at 1 h than that at 1 day after ISO treatment, including up-regulation of *Il1b*, *Il6*, and other inflammatory factors (Fig. 1f–h). For PE treatment, the number of differentially expressed genes kept increasing over time (Fig. 1i–k). In addition, within these differentially expressed genes, the fold changes of some reported inflammatory factors such as *Nlrp3*, *Il1b*, *Il6*, and *Il18* also rise over time. In summary, ISO induced a transient pulse in the transcriptome that recovered within one day. In contrast, PE induced sustained transcriptome changes, particularly in inflammatory response.

Changes in gene expression over time were closely associated with inflammation

To further elucidate biological processes associated with the differential responses, we compared the functional enrichments of all sets of genes according to their patterns of fold changes during ISO and PE treatment.

At 1 h after treatment, genes that were specifically upregulated under ISO treatment did not show a significant association with inflammation, but were mainly involved in angiogenesis (Supplementary Fig. 1). Contrarily, gene ontology (GO) analysis showed that the genes specifically up-regulated under PE treatment (Fig. 2a, orange area) were mostly involved in chemokine-mediated signaling pathways and leukocyte migration, particularly neutrophils (Fig. 2b). Meanwhile, genes upregulated by both ISO and PE treatments (Fig. 2a, blue area) were mainly involved in inflammation-related pathways (Fig. 2c), consistent with previous studies [16, 25]. In addition, the specifically downregulated genes under ISO treatment were primarily involved in the cellular response to external stimuli and virus infection (Supplementary Fig. 2a-c), while the small number of specifically downregulated genes under PE treatment did not associate with significant functional enrichment.

On 1 day after treatment, there were only a few differentially expressed genes induced by ISO, mostly unannotated (Supplementary Fig. 2d, e), consistent with the pulse-like dynamics under ISO treatment. By contrast, there were a large number of genes differentially expressed after PE treatment (Fig. 2d). Among these genes, those specifically up-regulated by PE (but not ISO) are predominantly involved in inflammatory-related pathways (Fig. 2e). Of note, the neutrophil extracellular trap formation pathway, a key pathway for neutrophils activities, was also substantially enriched in GO analysis. Meanwhile, the genes specifically down-regulated by PE (but not ISO) were predominantly engaged in metabolic processes (Fig. 2f). In summary, consistent with their patterns of global transcriptome changes, both ISO and PE stimulated the cardiac inflammatory pathway 1 h after treatment. However, ISO-induced cardiac inflammatory response returned to the baseline one day after treatment, whereas PE-induced inflammatory responses lasted at least one day. In addition, one day after PE treatment, metabolic pathways were significantly downregulated. Notably, GO analysis suggested that PE treatment may result in neutrophil infiltration, a phenomenon that did not occur under ISO treatment.

PE treatment led to neutrophil infiltration

Both macrophages and neutrophils are important responders to cardiac stress. According to previous reports, macrophages are one of the primary types of infiltrated cells in the heart during adrenergic receptor activation [26]. During the acute phase of inflammation, neutrophils are one of the first responders of inflammatory cells to migrate toward the site of inflammation [27, 28]. Therefore, to verify the hypothesis of PE-specific neutrophil infiltration inferred from RNA-Seq, we performed immunohistochemistry at various time points after ISO and PE treatments. First, macrophages were identified by the CD68 marker, by which we observed comparable infiltration of macrophages one day after both ISO and PE treatment (Fig. 3a-b).

Next, we labeled the neutrophils with marker Ly6G. Consistent with the RNA-Seq analysis, mouse heart tissue exhibited no neutrophil infiltration under ISO treatment (Fig. 3c, d). Meanwhile, we observed strong neutrophil infiltration one day after PE treatment (Fig. 3c). Seven biological replicates confirmed substantial neutrophil infiltration only on day 1 under PE treatment (Fig. 3d). Thus, it is confirmed that ISO treatment did not result in neutrophil infiltration throughout, whereas PE treatment resulted in significant neutrophil infiltration at one day.

Different expression patterns of chemokines affected neutrophil infiltration

Next, we searched the upstream pathways of inflammatory responses for factors linked to PE-specific neutrophil infiltration. Chemokines are a family of chemoattractant cytokines interacting with chemokine receptors on leukocytes to stimulate their directional movement [29]. We compared the RNA-Seq expression levels of all chemokines and chemokine receptors under different treatments. It was observed that the expression of chemokines under PE treatment was substantially higher than that under ISO treatment, and reached a maximum one day after PE treatment (Fig. 4a, left panel). Several of these chemokines were known to be associated with neutrophil migration, such as *Ccl24*, *Cxcl3*, *Cxcl5*, *Cxcl2*, *Ccl9*, *Ccl7*, *Cxcl1*, etc [30]. In addition, the expression of chemokine receptors was also much higher under PE treatment

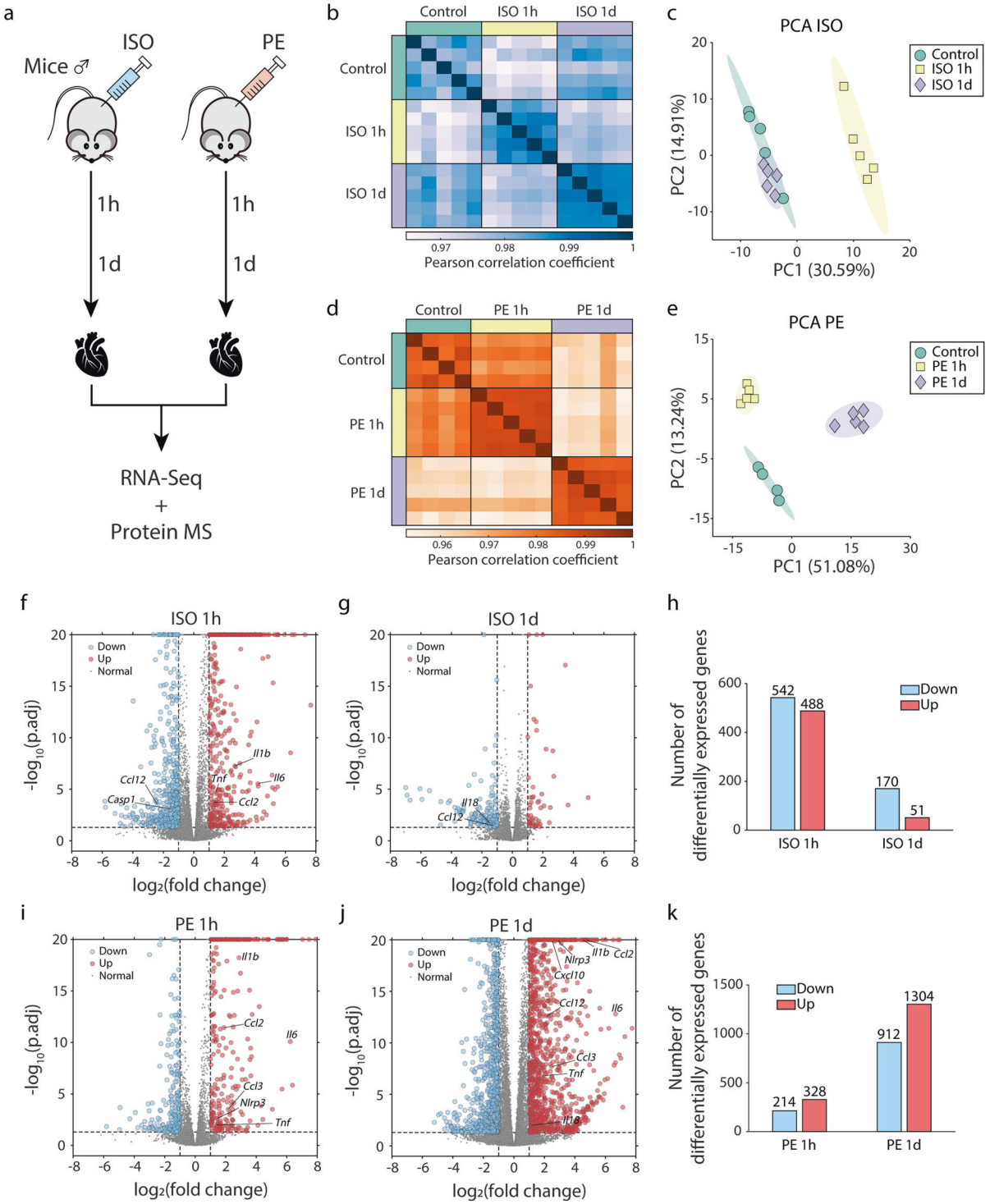

Fig. 1 The differences in transcriptional expression patterns between β-AR agonist (ISO) and α_1-AR agonist (PE) treatment. a Overview of experimental design. Five biological replicates were generated for each point in time, except for the control group in PE stimulation (four replicates). Mouse heart tissue was extracted for subsequent RNA sequencing and proteomics. **b** Heatmaps of Pearson correlation coefficients of RNA-seq for replicates under ISO treatment ($n = 5$, 5, and 5 for control, 1 h, 1d, respectively). **c** Principal-component analysis (PCA) of gene expressions from RNA-Seq under ISO treatment. **d-e** Same as **b**, **c**, but showing the results under PE treatment ($n = 4$, 5, and 5 for control, 1 h, 1d, respectively). The volcano plot showing the $\log_2$(RNA-Seq fold change) between ISO treatment and control, for 1 h (**f**) and 1 day (**g**) after treatment. **h** Numbers of differentially expressed genes at 1 h and 1 day after ISO treatment. **i–k** Same as (**f–h**), but showing the results from PE treatment.

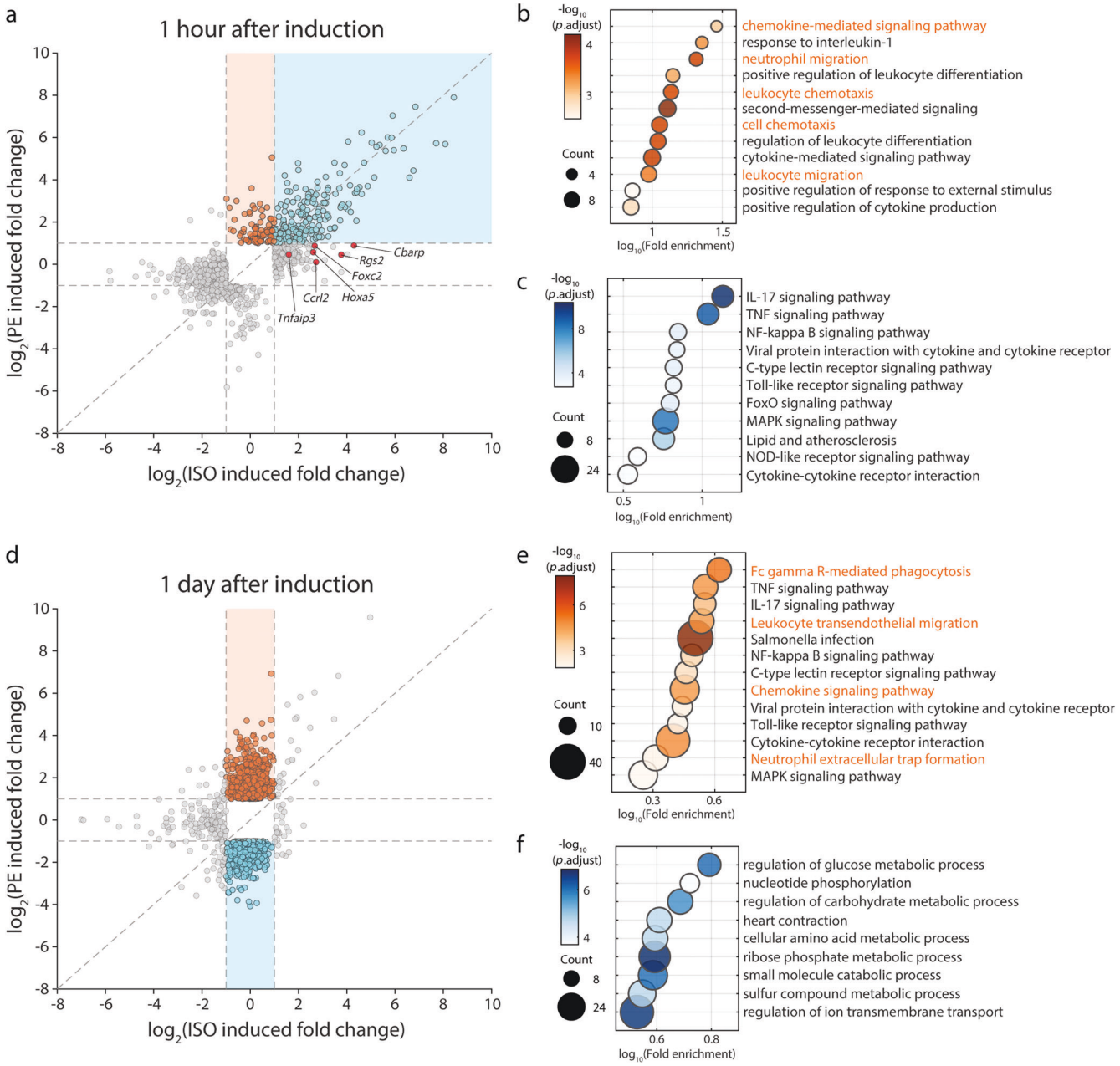

Fig. 2 Functional enrichment analysis of differentially expressed genes in time series after ISO and PE treatment. a Comparison of RNA-Seq fold change at 1 h after ISO ($n = 5$, 5, and 5 for control, 1 h, 1d, respectively) and PE treatments ($n = 4$, 5, and 5 for control, 1 h, 1d, respectively). Genes differentially expressed with statistical significance were shown. The genes highlighted in orange were specifically up-regulated under PE treatment but not under ISO, while those highlighted in blue were up-regulated under both ISO and PE. **b** Gene ontology (GO) enrichment analysis of genes specifically upregulated under PE treatment (orange in **a**). The color of the dots represents the $-\log_{10}$(adjusted *P* value), and the size represents the number of genes. GO BP terms with adjusted *P* value less than 0.05 are shown. **c** Same as **b**, but for genes up-regulated under both PE and ISO (blue in **a**). **d–f** Same as **a–c**, but showing the results 1 day after treatments, and genes highlighted in orange were specifically up-regulated under PE treatment, while those highlighted in blue were specifically downregulated under PE treatment.

than under ISO treatment, especially Cxcr2, a major chemokine receptor on neutrophils (Fig. 4a, right panel) [31, 32]. GSEA and KEGG Pathview analysis showed that the neutrophil extracellular trap pathway was significantly activated 1 day after PE treatment (Fig. 4b, and Supplementary Fig. 3). Furthermore, qPCR validation of *Cxcr2* confirmed that PE stimulated the expression of *Cxcr2*, which reached its peak at 1 day. Meanwhile, the expression of *Cxcr2* under ISO treatment remained low over time (Fig. 4c). These results suggested that the PE-induced infiltration of inflammatory cells, especially neutrophils, was partly attributable to stronger chemokine expressions.

We noticed in the RNA-Seq profile that after ISO treatment specifically, some chemokines were up-regulated at 1 h, then returned to their baseline levels at 1 day (Fig. 4a). It is intuitive to hypothesize that there may be genes that reduced inflammation under ISO treatment (Fig. 4d). Indeed, multiple genes specifically up-regulated at 1 h after ISO treatment were typically reported to inhibit inflammation, including *Tnfaip3* [33], *Ccrl2* [34], *Hoxa5* [35],

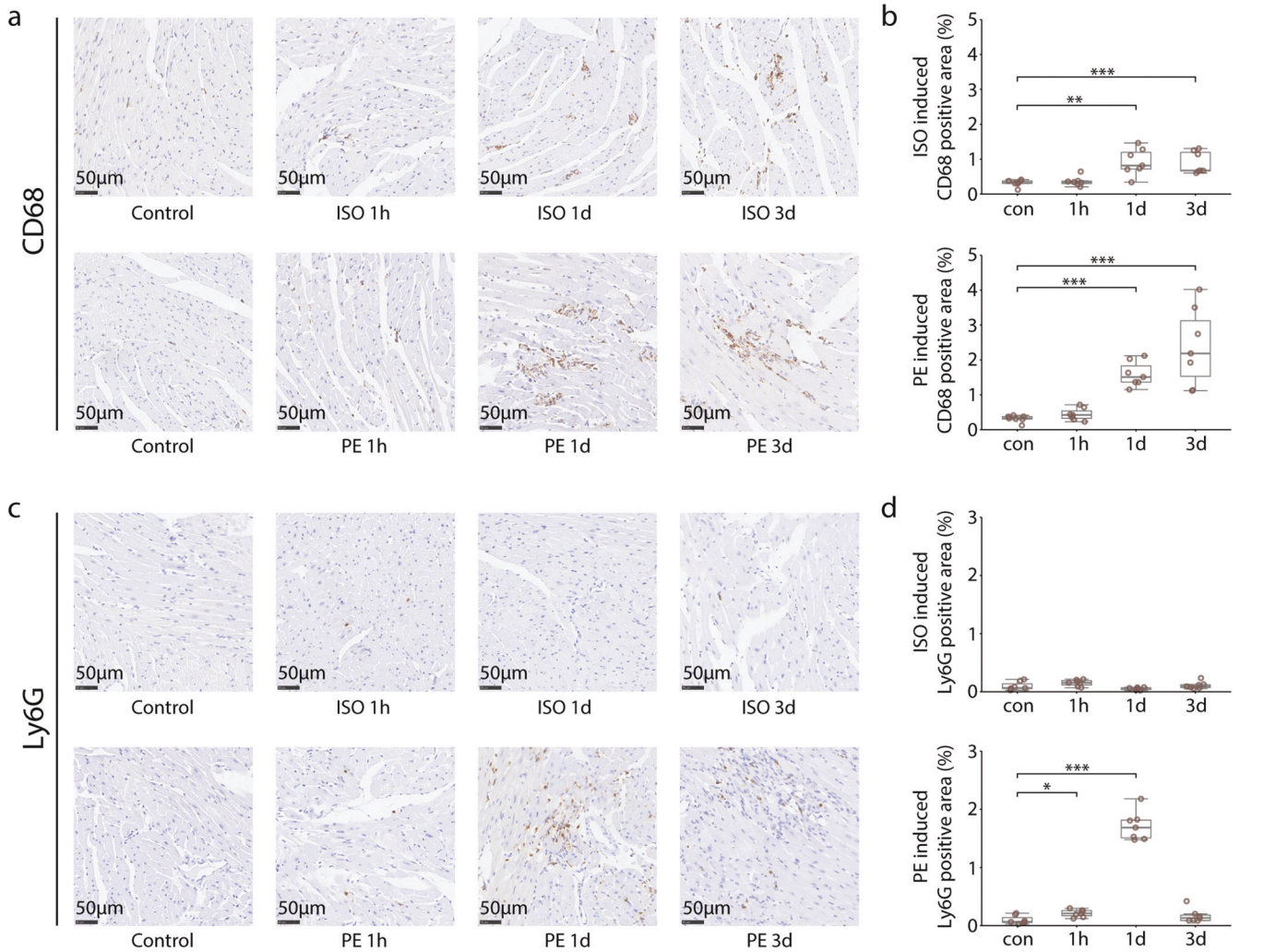

Fig. 3 Differences between the inflammatory cell infiltration induced by ISO and PE. a Immunostainings of CD68 (macrophage marker) in the heart at different time points after treatment ($n = 7$). **b** Statistics on macrophage infiltration areas at different time points after ISO (up panel) and PE (down panel) treatment, corresponding to the two panels in **a**. **c** Immunostainings of Ly6G (neutrophil marker) in the heart at different time points after treatment ($n = 7$). **d** Statistics on neutrophil infiltration areas at different time points after ISO (up panel) and PE (down panel) treatment, corresponding to the two panels in **c**. For all statistical plots, ANOVA was performed to test for statistical significance. "*" represents *P* value less than 0.05. "**" represents *P* value less than 0.01. "***" represents *P* value less than 0.001.

Foxc2 [36], *Rgs2* [37], and *Cbarp* [38, 39] (Fig. 2a). Especially, *Rgs2* plays an anti-inflammatory role and inhibits neutrophils [37], and the loss of *Ccrl2* leads to a stronger inflammatory response [34]. qPCR validations demonstrated that both *Rgs2* and *Ccrl2* were considerably upregulated 1 h after ISO treatment, but largely unaffected by PE treatment (Fig. 4e,f). In conclusion, we discovered that ISO resulted in the expression of inflammatory suppressor genes at 1 h, which may account for lower chemokine expression, weaker inflammatory cell infiltration, and reduced inflammation responses one day after treatment.

PE-induced inflammatory response through activating the NF-κB pathway

The aforementioned investigation revealed that PE treatment led not only to the infiltration of neutrophils, but also a stronger and more persistent inflammatory response. Regarding the NOD-like receptor signaling pathway and cytokine-cytokine receptor interaction pathway, two important pro-inflammation pathways, KEGG Pathview showed that PE-induced activation led to upregulation of a greater number of pathway-associated genes than ISO-induced activation (Supplementary Figs. 4, 5). To further explore the mechanisms behind the distinct inflammatory responses induced by ISO and PE treatment, we focused on the NF-κB signaling pathway. NF-κB is a pivotal mediator of inflammatory response, inducing the expression of various inflammatory genes and participating in inflammasome regulation [40]. GSEA analysis showed that the NF-κB signaling pathway was significantly activated at 1 day induced by PE, but not by ISO (Fig. 5a, and Supplementary Fig. 6). Then, we performed qPCR validations on the inflammatory factors downstream of NF-κB. It is worth noting that there were substantial neutrophil infiltration and *Cxcr2* upregulation only at day 1 after PE treatment (Figs. 3d, 4c). To verify whether the expression peak of inflammatory genes after PE treatment was at day 1, we extended the sampling time point of qPCR validation to day 3. It showed that *Tnf*, *Il6*, *Il18*, and *Il1b* were significantly up-regulated from 1 h to 1 day after PE, but not ISO treatment (Fig. 5b). And the expression of these genes dropped significantly at day 3 after PE treatment, indicating that the expression of inflammatory genes peaked at day 1 after PE treatment.

The phosphorylation of P65, a core protein in NF-κB pathway, is critical for nuclear localization of NF-κB and initiation of transcription of downstream target genes [41]. Therefore, we performed Western blot analysis on the phosphorylation level of

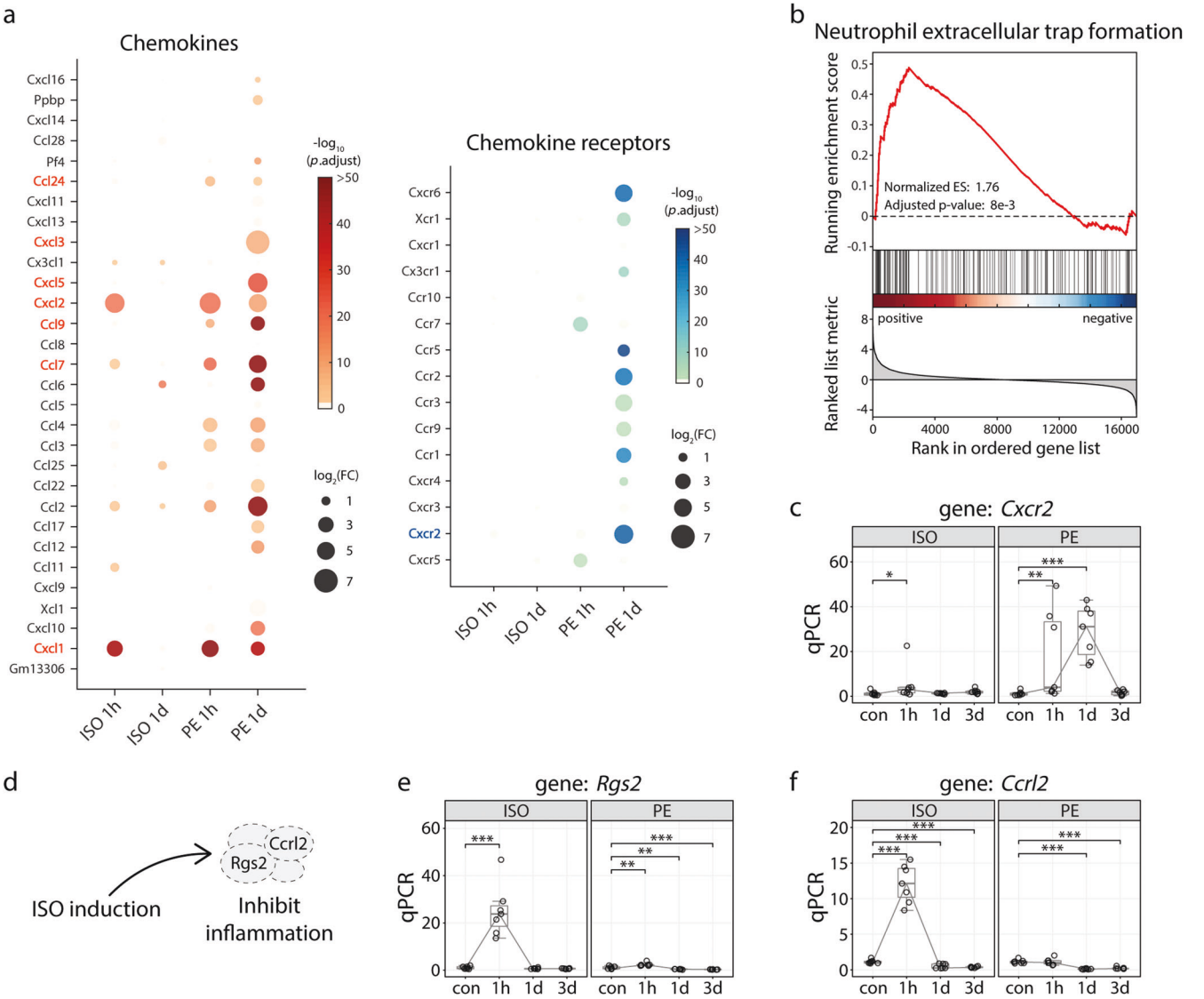

Fig. 4 Expression analysis of genes associated with neutrophils after ISO and PE treatment. a Comparison of mRNA levels of chemokine (left panel) and chemokine receptor (right panel) under different experimental conditions. The color of the dots represents the $-\log_{10}$(adjusted *P* value), and the size represents the $\log_2$(RNA-Seq fold change). Chemokines and chemokine receptors related to neutrophils are highlighted. **b** Gene set enrichment analysis (GSEA) of neutrophil extracellular trap formation pathway genes at 1 day after PE treatment. RNA-Seq fold changes were estimated with DESeq2. Genes were sorted according to their $\log_2$(fold change). **c** Quantitative real-time PCR (qPCR) analysis for gene *Cxcr2* ($n = 7$). **d** Illustration of ISO treatment activates genes inhibiting inflammation, including Rgs2 and Ccrl2. **e, f** Quantitative real-time PCR (qPCR) analysis for genes *Rgs2* and *Ccrl2* ($n = 7$). For all qPCR analyses, ANOVA was performed to test for statistical significance. "*" represents *P* value less than 0.05. "**" represents *P* value less than 0.01. "***" represents *P* value less than 0.001.

P65. The results showed that the proportion of phosphorylated P65 did not increase after ISO treatment (Fig. 5c), but increased significantly after PE treatment (Fig. 5d). In summary, combined with downstream genes analysis of NF-κB, we revealed that PE treatment activated the NF-κB signaling pathway, which may be attributable for the strong and persistent inflammatory response.

Furthermore, to further validate the effects of NF-κB pathway, we pretreated the mice with NF-κB inhibitor Bay11-7082 before PE treatment. We found that inhibition of NF-κB could effectively suppress the upregulation of these inflammatory genes induced by PE treatment (Fig. 6a). Remarkably, immunostaining experiments confirmed that inhibition of NF-κB pathway significantly reduced the infiltration of macrophages and neutrophils induced by PE treatment at 1 day (Fig. 6b–e). These results further established that PE treatment activated inflammatory response through NF-κB pathway.

Transcriptome and proteome changed in concert during cardiac inflammation

The aforementioned transcriptome analysis revealed that PE treatment results in a more powerful and prolonged inflammatory response than ISO treatment. Next, we examined the correlation between mRNA and protein levels to check if this observation holds true at the proteomic level. After filtering out the low-expression proteins, a total of 2036 proteins under ISO treatment and 3255 proteins under PE treatment were used for subsequent analysis. Under ISO treatment, there were only 18 and 178 differentially expressed proteins by protein Mass Spectrometry (MS) at one hour and one day, respectively. Meanwhile, after PE treatment, these two numbers are about ten and five folds larger than those after ISO treatment (Fig. 7a). In addition, neither the transcriptome nor the proteome changed appreciably after ISO treatment, accompanied by low correlation coefficients between

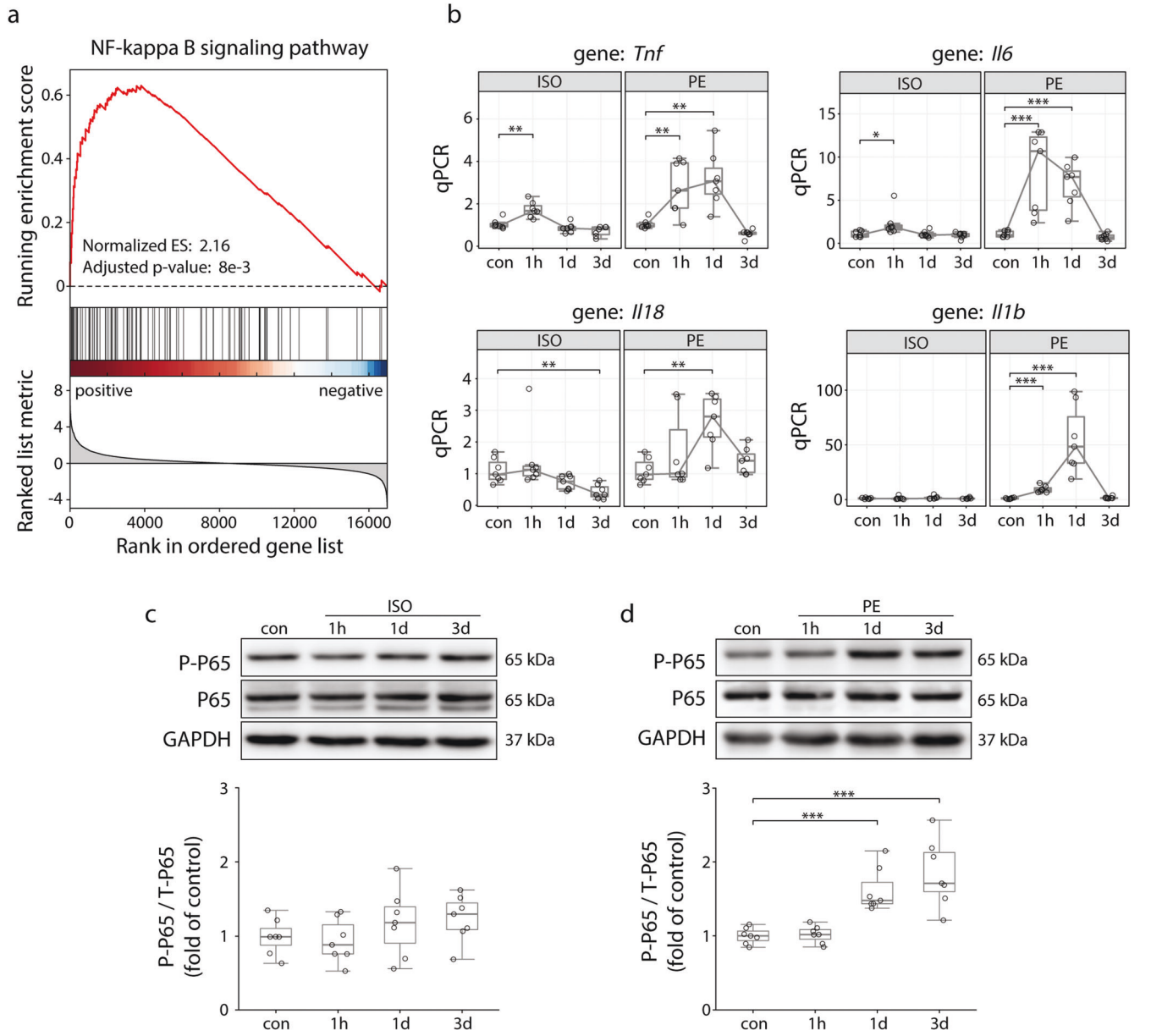

Fig. 5 PE treatment activates the NF-κB pathway. a Gene set enrichment analysis (GSEA) of NF-κB pathway genes at 1 day after PE treatment. RNA-Seq fold changes were estimated with DESeq2. Genes were sorted according to their $\log_2$(fold change). **b** Quantitative real-time PCR (qPCR) analysis for NF-κB downstream genes *Tnf*, *Il6*, *Il18*, *Il1b* ($n = 7$). Western blot analysis for P65, phosphorylated P65 (P-P65) in cardiac tissue under ISO (**c**) and PE (**d**) treatments ($n = 7$). For all qPCR and Western blot analyses, ANOVA was performed to test for statistical significance. "*" represents *P* value less than 0.05. "**" represents *P* value less than 0.01. "***" represents *P* value less than 0.001.

the fold changes (Fig. 7b, and Supplementary Fig. 7). Nevertheless, there was a significant correlation between the fold changes of mRNA and protein levels one day after PE treatment, with a correlation coefficient of 0.38 (Fig. 7c).

To identify whether differentially expressed proteins in the proteome are also associated with inflammatory responses, we selected the significantly up-regulated proteins one day after PE treatment with fold change >1.2 and adjusted *P* value < 0.05. Functional enrichment analysis showed that these genes were mainly involved in three types of biological processes, including inflammation and immunity, leukocyte migration, and response to oxidative stress (Fig. 7d, left panel). Furthermore, the mRNA and protein levels of the enriched genes in the corresponding GO terms were significantly up-regulated one day after PE treatment (Fig. 7d, right panel). We also selected the significantly downregulated proteins one day after PE treatment with fold change <−1.2 and adjusted *P* value < 0.05. Consistent with the results from RNA-Seq in Fig. 2f, these genes are primarily involved in energy-related metabolic processes such as TCA cycling and oxidative phosphorylation (Fig. 7e). In summary, the combined analysis of transcriptome and proteome confirmed that transcriptome and proteome changed in concert during cardiac inflammation 1 day after PE treatment.

In addition, to validate the expression changes observed in protein MS, we performed Western blot analysis for inflammation-related and metabolism-related genes that were significantly up- and downregulated, respectively. Results of Western blot further confirmed that PE treatment caused the upregulation of these inflammation-related genes as well as the downregulation of metabolism-related genes (Fig. 7f, g). We also measured the ATP

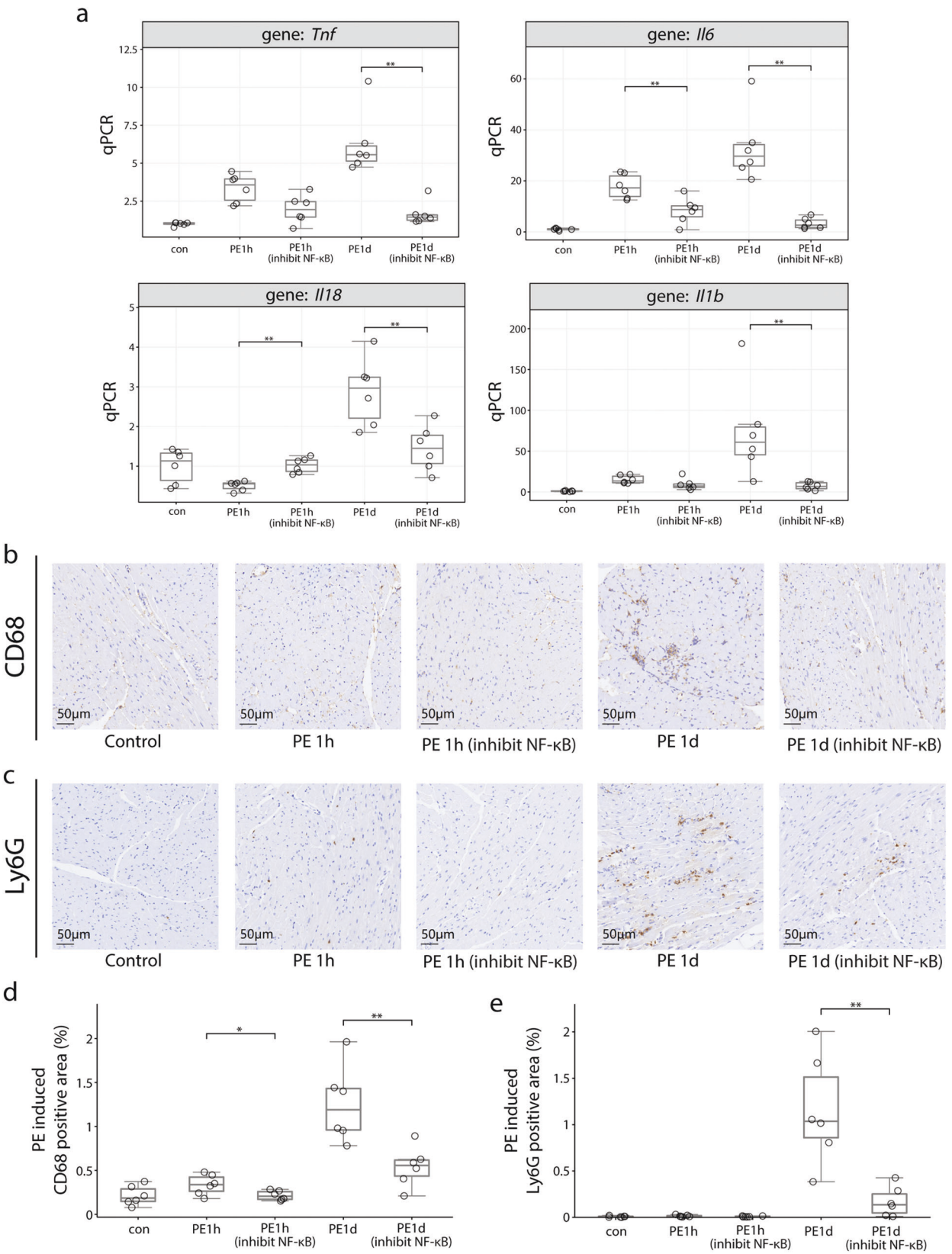

Fig. 6 Inhibition of NF-κB significantly reduced inflammatory response after PE treatment. a Quantitative real-time PCR (qPCR) analysis for NF-κB downstream genes *Tnf*, *Il6*, *Il18*, *Il1b* ($n = 6$). **b** Immunostainings of CD68 (macrophage marker) in the heart at different time points after treatment ($n = 6$). **c** Immunostainings of Ly6G (neutrophil marker) in the heart at different time points after treatment ($n = 6$). **d** Statistics on macrophage infiltration areas at different time points after PE treatment with and without NF-κB inhibitor. **e** Statistics on neutrophil infiltration areas at different time points after PE treatment with and without NF-κB inhibitor. For all statistical plots, ANOVA was performed to test for statistical significance. "*" represents *P* value less than 0.05. "**" represents *P* value less than 0.01. "***" represents *P* value less than 0.001.

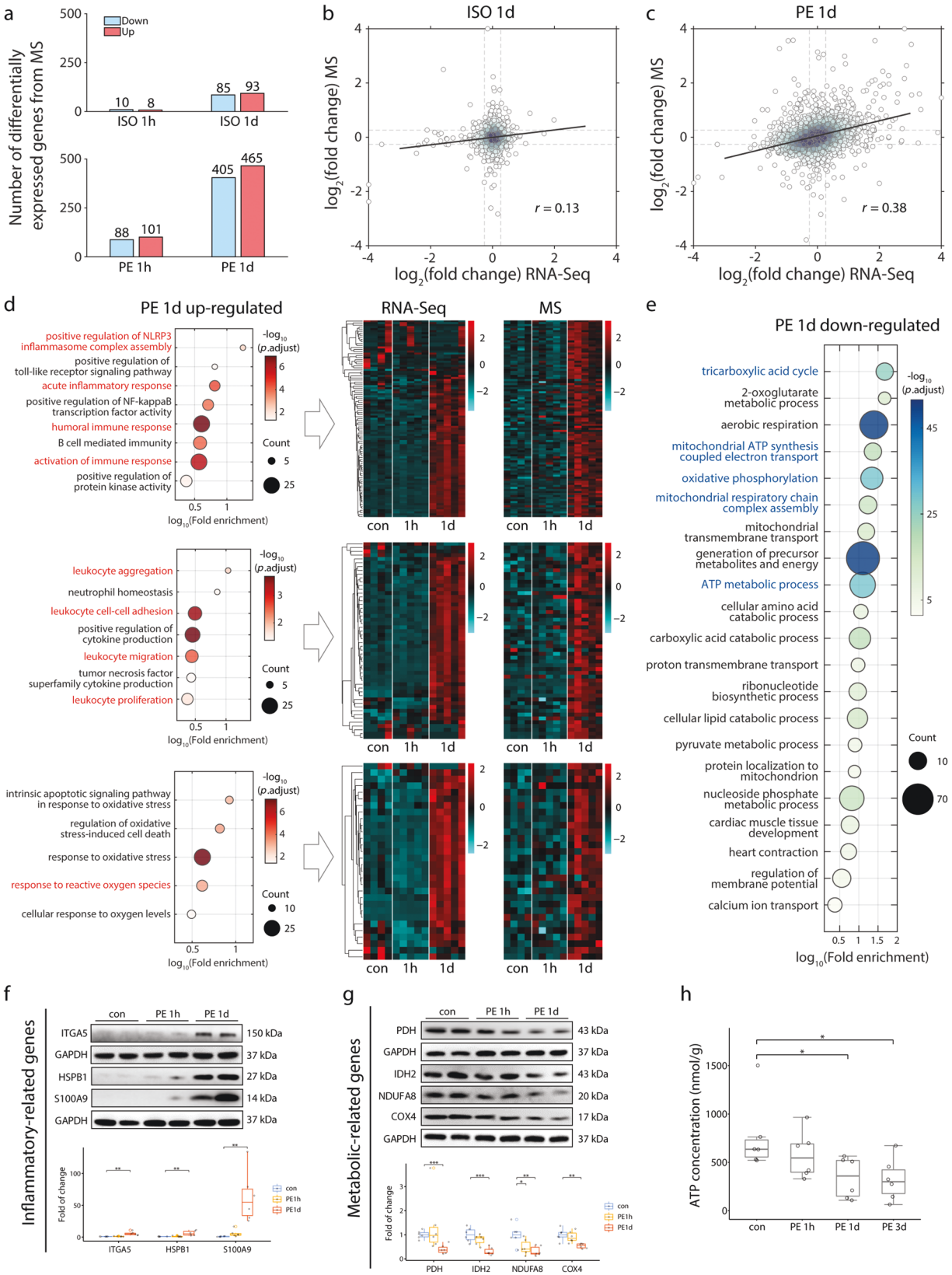

levels in the heart tissue. The cardiac ATP levels were significantly decreased on day 1 and day 3 after PE treatment, consistent with the results in transcriptome and proteome (Fig. 7h). In agreement, ATP generation-related proteins (NDUFA8 and COX4) decreased at day 1 after PE treatment (Fig. 7g). These results indicated that PE downregulated metabolic proteins and inhibited ATP generation. Moreover, we also detected the ROS levels in cardiac tissue after PE treatment using fluorescence staining. The results showed that

Fig. 7 Combined analysis of transcriptome and proteome after ISO and PE treatment. a Numbers of differentially expressed genes from protein MS at 1 h and 1 day after ISO (upper panel, $n = 5$, 5, and 5 for control, 1 h, 1d, respectively) and PE treatment (lower panel, $n = 4$, 5, and 5 for control, 1 h, 1d, respectively). **b** Comparison between RNA-Seq and protein-MS fold changes at 1 day after ISO treatment. Lines in the figure represent the linear fitting of all 2036 genes. **c** Comparison between RNA-Seq and protein MS fold changes at 1 day after PE treatment. The color of the dots represents the density. The lines in the figure represent the linear fitting of all 3255 genes. **d** Gene ontology (GO) enrichment analysis of upregulated genes from protein MS at 1 day after PE treatment (left panel), and heatmaps of mRNA (middle panel) and protein (right panel) expression levels for the corresponding enriched genes. The heatmap was Z-score normalized by row. Gene orders in RNA-Seq and MS were consistent. **e** Gene ontology (GO) enrichment analysis of downregulated genes from protein MS at 1 day after PE treatment. The color of the dots represents the $-\log_{10}$(adjusted P value), and the size represents the number of genes. GO BP terms with adjusted P value less than 0.05 are shown. Western blot analysis for inflammatory-related genes (**f**) and metabolism-related genes (**g**) in cardiac tissue after PE treatments ($n = 6$). **h** ATP concentration in cardiac tissue after PE treatment ($n = 6$). ANOVA was performed to test for statistical significance. "*" represents P value less than 0.05. "**" represents P value less than 0.01. "***" represents P value less than 0.001.

the ROS level increased at 1 h after PE treatment (Supplementary Fig. 8).

PE treatment resulted in the downregulation of energy-related metabolic processes

To further clarify the downregulation of metabolic processes one day after PE treatment, we compared the expression of typical genes in the TCA cycle (29 genes) and oxidative phosphorylation pathways (80 genes) across different conditions by both RNA-seq and MS. One day after PE treatment, the mRNA and protein levels of the genes in both pathways were down-regulated in concert, whereas ISO treatment had no discernible effect (Fig. 8a, b). Since both the TCA cycle and oxidative phosphorylation are important pathways for cell energy production [42], our findings suggested that PE treatment not only caused a strong inflammatory response at one day, but also altered the fundamental metabolism of cells.

To explore the link between cardiac inflammatory response and metabolic disorders, we compiled a list of inflammation and immune-related genes involved in immune response, inflammation-related signaling pathways, leukocyte migration, regulation of cytokine production and interaction, etc., that were significantly up-regulated in transcriptome and proteome after PE treatment. We also compiled metabolism-related genes that were significantly downregulated in transcriptome and proteome after PE treatment, involved in oxidative phosphorylation, ATP-related metabolic process, etc. In addition, we performed protein-protein association analysis for the two groups of genes [24]. There was a diversity of interactions between immune and metabolism-related genes, which constituted a relatively complex association network (Fig. 8c). These results offered valuable clues for future studies on the interplay between immune response and metabolic changes.

DISCUSSION

In this study, we systematically compared the effects of α_1-AR and β-AR acute overactivation in the heart. We found that both overactivation of α_1- and β-AR resulted in cardiac inflammation and continuous infiltration of macrophages from 1 day to 3 days after treatment, but the temporal transcriptional profiles exhibit substantial differences. The change in the transcriptional profile caused by β-AR activation transiently increased at 1 h and returned to baseline at 1 day. Whereas α_1-AR activation resulted in sustained expression of inflammatory genes. Intriguingly, the overactivation of α_1-AR led to neutrophil infiltration at 1 day after PE treatment, which was closely associated with the up-regulation of chemokines and the activation of NF-κB pathway. Furthermore, by integrating transcriptome and proteomics, we confirmed that PE treatment led to coordinated changes in mRNA and protein, and found that it even affected basic metabolic processes. These findings reveal profound differences in cardiac inflammation caused by α_1- and β-AR (Fig. 9).

In our findings, the temporal profiles of cardiac inflammation induced by ISO and PE differed drastically. ISO induced a pulse-like response, accompanied by a poor correlation between mRNA and protein changes. There may be two possible explanations for the poor correlation between mRNA and protein changes. First, previous studies suggested that besides changes in transcriptional level, some of the ISO-induced responses occur at the post-transcriptional level [16]. For example, the mRNA level of *Ccl2*, *Il6*, and *Tnf* after ISO treatment increased in this study, consistent with the ELISA result in the previous study, indicating a transcriptional regulation for these genes. In contrast, the ISO-induced cleavage activation of IL18 in heart by activating inflammasome, which directly increased the protein abundance of activated IL18 without increasing mRNA level [16]. Second, protein synthesis takes time. Thus, there was a delay between transcriptional induction and protein level changes [43]. In summary, the post-transcriptional regulation and temporal delay of protein synthesis may be accountable for the poor mRNA-protein correlation under ISO treatment. In comparison, PE induced more sustained transcriptional expression increase, resulting in a strong correlation between transcriptome and proteome changes at 1 day. This strong correlation suggested that cardiac responses to PE treatment are more at the transcriptional level. Activation of the NF-κB pathway may be one of the potential reasons for the different temporal profiles of PE treatment compared with ISO. The NF-κB pathway is known to up-regulate the expression of various inflammatory genes, including *Tnf* and *Il1b*, which can further activate the NF-κB pathway, tending to form positive feedbacks that amplify inflammatory responses. Consistent with our results, a recent study showed that combined chronic α_1-AR + β-AR stimulation led to more inflammation than β-AR stimulation alone [44].

The final inflammatory state depends on the balance between damage and repair [45]. Transcriptomic analysis showed that the transcription of inflammatory genes induced by ISO returned to baseline at 1 day. In addition to the fact that ISO treatment does not activate the NF-κB pathway, it is also important to note that ISO treatment can promote cardiac repair to some extent. In our study, ISO treatment led only to macrophage infiltration, which was consistent with previous studies [16]. Beyond stimulating immune system, macrophages themselves play a significant anti-inflammatory role [46, 47]. Moreover, ISO treatment led to specific up-regulation of genes involved in promoting repair or inhibiting inflammation at 1 h (Supplementary Fig. 1), particularly *Rgs2* and *Ccrl2*. They play a crucial role in regulating immune responses [48, 49]. And knockdown of either *Rgs2* or *Ccrl2* has been reported to lead to increased inflammation [34, 37, 50].

The roles of α_1- and β-AR activation in the heart depend on the disease state. For example, the activation of α_1-AR induced by PE plays a protective role in severe infections such as sepsis [51]. However, in the absence of exogenous strong proinflammatory effects, overactivation of α_1- and β-AR can lead to harmful cardiac inflammation. Previous reports also indicated that PE treatment-induced cardiac hypertrophy [52–54]. In our study, contrary to ISO treatment, we found that PE treatment resulted in additional neutrophil infiltration at 1 day, which had not been reported in previous studies. Neutrophil has been suggested to play a causal

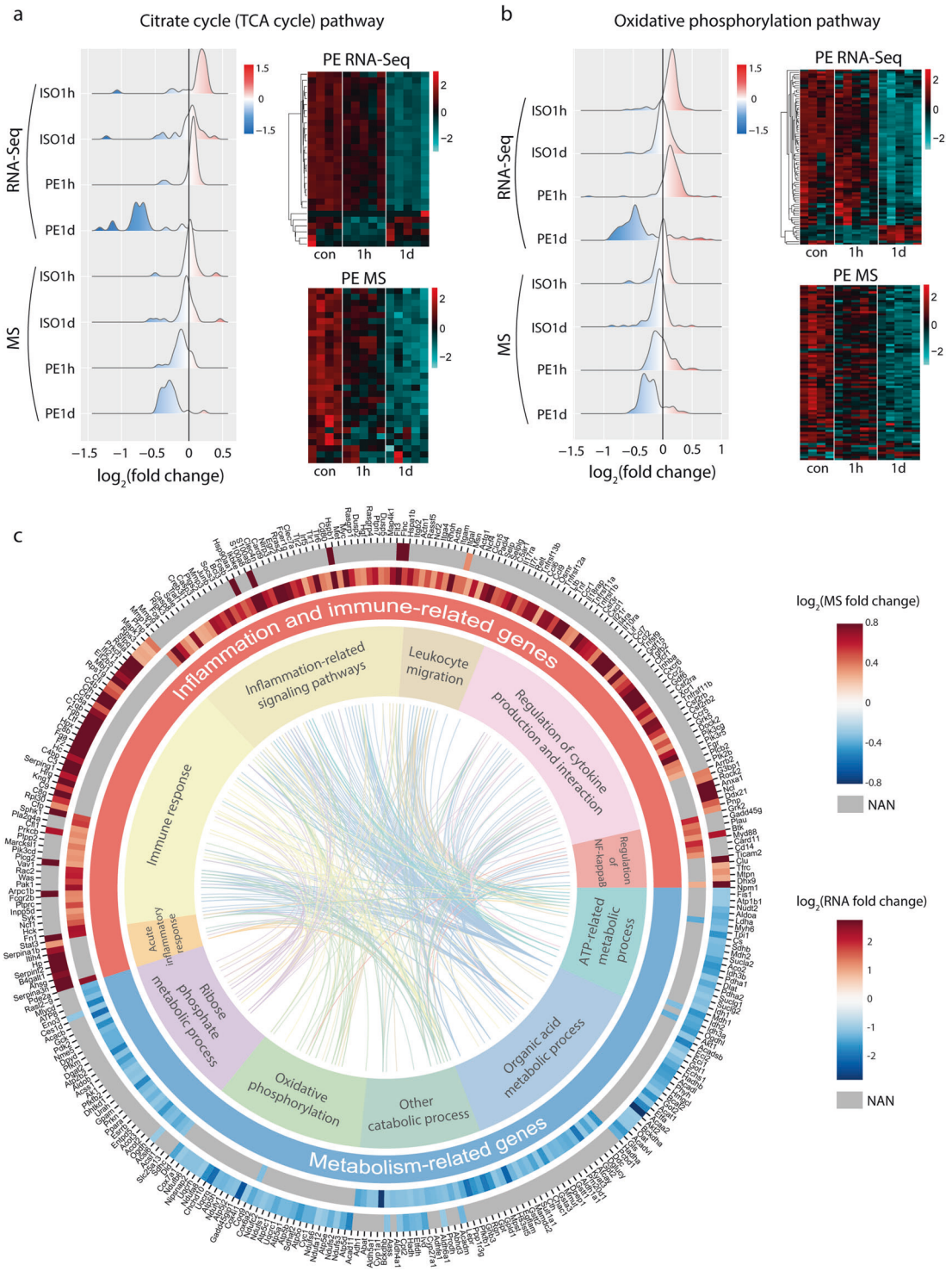

Fig. 8 PE causes metabolic pathway downregulation. a RNA-Seq and protein MS fold change distribution of genes in the citrate cycle (TCA cycle) pathway. The right panels are heatmaps of mRNA and protein expression levels for the corresponding genes under PE treatment. The heatmap was Z-score normalized by row. Gene orders in RNA-Seq and MS were consistent. All 29 genes measured in our data are shown. **b** Same as **a** but showing results from the oxidative phosphorylation pathway. All 80 genes measured in our data are shown. **c** The association between inflammation and metabolism-related genes that were significantly regulated in our study. The outermost track represented the log_2(MS fold change) and the sub-outer track represented the log_2(RNA fold change). The innermost track represented functional enrichment of genes. The internal links represented protein-protein associations from STING database between pairs of genes.

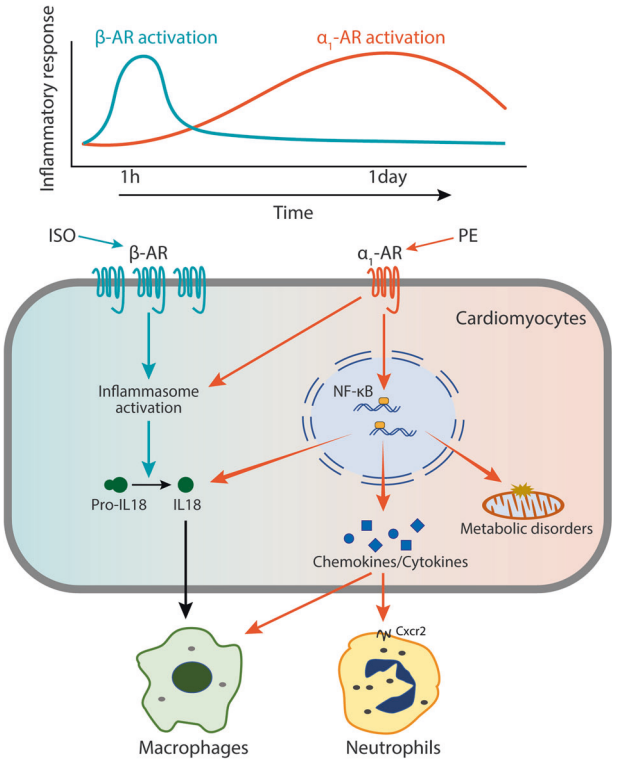

Fig. 9 Illustration of the differences in inflammatory responses between α_1-AR and β-AR activation. α_1- and β-AR activations induced sustained and transient inflammatory gene expression, respectively. The overactivation of β-AR induced the cleavage activation of IL18 by activating inflammasome, while the overactivation of α_1-AR led to neutrophil infiltration at 1 day, which was closely associated with the up-regulation of chemokines, activation of NF-κB pathway, and sustained inflammatory response. Furthermore, there are more metabolic disorders under α_1-AR overactivation compared with β-AR overactivation.

role in inflammatory monocyte/macrophage recruitment, thereby promoting the development of inflammation [55]. In addition, early after myocardial infarction, neutrophil infiltration in the heart is frequently observed [56]. Therefore, we hypothesized that neutrophil infiltration induced by PE may be associated with persistent inflammation. Considering that neutrophil infiltration, chemokine receptor *Cxcr2* expression, and downstream genes of NF-κB pathway all reached their peak at day 1, we inferred that the inflammatory response after PE treatment reached its peak at the same time.

The downregulation of mitochondrial metabolism pathways, including the citrate cycle pathway and the oxidative phosphorylation pathway, is another characteristic phenomenon following PE treatment. The downregulation is consistent in both transcriptomic and proteomic levels, implying PE treatment may cause more metabolic disorders. Indeed, the tight association between inflammation and metabolism has been suggested in the heart [57]. Metabolic disorders can be caused by abnormal accumulation of metabolites, which directly influence inflammatory responses. For example, metabolic intermediates, such as succinate, are accumulated during the disorder of the citrate cycle and promote the expression of proinflammatory IL-1β via the hypoxia-inducible factor 1α pathway [58]. In addition, oxidative phosphorylation is the main process in cardiomyocytes producing ATP, and it also generates reactive oxygen species (ROS) that induce inflammation [59]. Previous studies have reported that ROS generation was enhanced following α-AR stimulation. In adult rat cardiac myocytes, α_1-AR stimulation induces NAD(P)H oxidase-depended ROS generation, leading to the activation of the Ras-Raf-MEK1/2-ERK1/2 pathway in vitro, and resulting in myocyte hypertrophy [60, 61]. In this study, we found ROS levels in cardiac tissue were also elevated after PE treatment in vivo, which may contribute to cardiac inflammation (Supplementary Fig. 8). In this study, pathways related to ROS were significantly upregulated after PE treatment. Excessive ROS promotes the production of inflammatory cytokines and activates the NLRP3 inflammasome, thereby contributing to inflammation [62]. Moreover, damage-associated molecules can be released from damaged mitochondria and activate Toll-like receptors or NLRP3 inflammasomes to initiate inflammatory signaling [63]. In summary, the metabolic disorder following PE treatment may further amplify the cascade of cardiac inflammation.

One limitation of our study is that proteomics cannot reach the same width of the genome as transcriptomics because of the high expression of mitochondria-related genes in cardiomyocytes and the high detection line of proteomics. The connection between acute cardiac inflammation and metabolic disorders calls for further investigation using a combination of metabolomics and computational techniques. Both β-AR and α_1-AR have cardioprotective and cardiotoxic effects. Further studies are needed to find the strategy promoting the protective effects of AR signaling while minimizing cardiotoxic effects. To achieve this goal, it is important to understand the contribution of different types of cells to cardiac inflammation upon sympathetic stress. Cardiac inflammation is associated with a variety of cell types, including immune cells, cardiac myocytes, fibroblasts and endothelial cells [64]. The bulk sequencing of heart tissue used in our study cannot distinguish the effects of different types of cells, thus single-cell transcriptomics is needed in the future studies. Despite of the limitation, our findings elucidated the similarities and differences in cardiac inflammation caused by acute α_1- and β-AR overactivation, thus providing novel strategies and potential targets for clinical treatment of stress-associated cardiovascular diseases. In fact, in the typical disease of stress-induced heart injury, such as stress cardiomyopathy with high mortality [65], treatment with β-blocker in the acute phase did not reduce mortality [66], implying that inhibition of β-AR is not sufficient to ameliorate stress-induced heart injury. Therefore, our findings suggested that besides using β-blocker as soon as possible, blocking α_1-AR within one day after stress should also be considered for the treatment of acute stress associated cardiovascular diseases.

DATA AVAILABILITY

The RNA-seq data are available in the GEO database with accession number GSE211134. The mass spectrometry proteomics data have been deposited to the ProteomeXchange Consortium via the PRIDE [67] partner repository with the dataset identifier PXD036011.

ACKNOWLEDGEMENTS

This work was supported by the Beijing Municipal Natural Science Foundation [grant number 7191013 to EDD], the National Key R&D Program of China [2021YFF0501401 to HX; 2021YFF1200500 to ZYL], the National Natural Science Foundation of China [grant numbers 82030072, 81822003 to HX; 81830009 to YYZ; 82100280 to JMW], the Haihe Laboratory of Cell Ecosystem Innovation Fund [grant number HH22KYZX0047 to EDD], and the Key Clinical Projects of Peking University Third Hospital [grant number BYSYZD2019022 to HX]. This work was partly supported by grants from Peking-Tsinghua Center for Life Sciences.

AUTHOR CONTRIBUTIONS

HX and JMW conceived and designed the research; MMZ, DZ, and JMW performed the research; DZ performed the data curation and formal analysis; RW and YBX helped with the experiments; GX and JQS helped with the data analysis; DZ, JMW, HX,

and ZYL wrote and edited the manuscript; HX, ZYL, YYZ, and EDD supervised the Project. All authors approved the manuscript.

ADDITIONAL INFORMATION

Supplementary information The online version contains supplementary material available at https://doi.org/10.1038/s41401-022-01048-5.

Competing interests: The authors declare no competing interests.

REFERENCES

1. Scott-Solomon E, Boehm E, Kuruvilla R. The sympathetic nervous system in development and disease. Nat Rev Neurosci. 2021;22:685–702.
2. Hering D, Lachowska K, Schlaich M. Role of the sympathetic nervous system in stress-mediated cardiovascular disease. Curr Hypertens Rep. 2015;17:80.
3. O'Connell TD, Jensen BC, Baker AJ, Simpson PC. Cardiac alpha1-adrenergic receptors: novel aspects of expression, signaling mechanisms, physiologic function, and clinical importance. Pharmacol Rev. 2014;66:308–33.
4. Kivimäki M, Steptoe A. Effects of stress on the development and progression of cardiovascular disease. Nat Rev Cardiol. 2018;15:215–29.
5. Jensen BC, O'Connell TD, Simpson PC. Alpha-1-adrenergic receptors in heart failure: the adaptive arm of the cardiac response to chronic catecholamine stimulation. J Cardiovasc Pharmacol. 2014;63:291–301.
6. Wachter SB, Gilbert EM. Beta-adrenergic receptors, from their discovery and characterization through their manipulation to beneficial clinical application. Cardiology. 2012;122:104–12.
7. Baker AJ. Adrenergic signaling in heart failure: a balance of toxic and protective effects. Pflug Arch. 2014;466:1139–50.
8. do Vale GT, Ceron CS, Gonzaga NA, Simplicio JA, Padovan JC. Three generations of β-blockers: history, class differences and clinical applicability. Curr Hypertens Rev. 2019;15:22–31.
9. Wright JM, Musini VM, Gill R. First-line drugs for hypertension. Cochrane Database Syst Rev. 2018;4:Cd001841.
10. Myagmar BE, Flynn JM, Cowley PM, Swigart PM, Montgomery MD, Thai K, et al. Adrenergic receptors in individual ventricular myocytes: the Beta-1 and Alpha-1B are in all cells, the Alpha-1A is in a subpopulation, and the Beta-2 and Beta-3 are mostly absent. Circ Res. 2017;120:1103–15.
11. Motiejunaite J, Amar L, Vidal-Petiot E. Adrenergic receptors and cardiovascular effects of catecholamines. Ann Endocrinol. 2021;82:193–7.
12. Vonderlin N, Siebermair J, Kaya E, Köhler M, Rassaf T, Wakili R. Critical inflammatory mechanisms underlying arrhythmias. Herz. 2019;44:121–9.
13. Ong SB, Hernández-Reséndiz S, Crespo-Avilan GE, Mukhametshina RT, Kwek XY, Cabrera-Fuentes HA, et al. Inflammation following acute myocardial infarction: Multiple players, dynamic roles, and novel therapeutic opportunities. Pharmacol Ther. 2018;186:73–87.
14. Murphy SP, Kakkar R, McCarthy CP, Januzzi JL Jr. Inflammation in heart failure: JACC state-of-the-art review. J Am Coll Cardiol. 2020;75:1324–40.
15. Singh T, Khan H, Gamble DT, Scally C, Newby DE, Dawson D. Takotsubo syndrome: pathophysiology, emerging concepts, and clinical implications. Circulation. 2022;145:1002–19.
16. Xiao H, Li H, Wang JJ, Zhang JS, Shen J, An XB, et al. IL-18 cleavage triggers cardiac inflammation and fibrosis upon β-adrenergic insult. Eur Heart J. 2018;39:60–9.
17. Xin JZ, Wu JM, Hu GM, Gu HJ, Feng YN, Wang SX, et al. α(1)-AR overactivation induces cardiac inflammation through NLRP3 inflammasome activation. Acta Pharmacol Sin. 2020;41:311–8.
18. Kim D, Langmead B, Salzberg SL. HISAT: a fast spliced aligner with low memory requirements. Nat Methods. 2015;12:357–60.
19. Love MI, Huber W, Anders S. Moderated estimation of fold change and dispersion for RNA-seq data with DESeq2. Genome Biol. 2014;15:550.
20. Yu G, Wang LG, Han Y, He QY. clusterProfiler: an R package for comparing biological themes among gene clusters. OMICS: A J Integr Biol. 2012;16:284–7.
21. Cox J, Hein MY, Luber CA, Paron I, Nagaraj N, Mann M. Accurate proteome-wide label-free quantification by delayed normalization and maximal peptide ratio extraction, termed MaxLFQ. Mol Cell Proteom. 2014;13:2513–26.
22. Bruderer R, Bernhardt OM, Gandhi T, Miladinović SM, Cheng LY, Messner S, et al. Extending the limits of quantitative proteome profiling with data-independent acquisition and application to acetaminophen-treated three-dimensional liver microtissues. Mol Cell Proteom. 2015;14:1400–10.
23. Tie L, Xiao H, Wu DL, Yang Y, Wang P. A brief guide to good practices in pharmacological experiments: Western blotting. Acta Pharmacol Sin. 2021;42:1015–7.
24. Szklarczyk D, Gable AL, Lyon D, Junge A, Wyder S, Huerta-Cepas J, et al. STRING v11: protein-protein association networks with increased coverage, supporting functional discovery in genome-wide experimental datasets. Nucleic Acids Res. 2019;47:D607–d13.
25. Xin JZ, Wu JM, Hu GM, Gu HJ, Feng YN, Wang SX, et al. α1-AR overactivation induces cardiac inflammation through NLRP3 inflammasome activation. Acta Pharmacol Sin. 2020;41:311–8.
26. Lafuse WP, Wozniak DJ, Rajaram MVS. Role of cardiac macrophages on cardiac inflammation, fibrosis and tissue repair. Cells. 2020;10:51.
27. De Larco JE, Wuertz BR, Furcht LT. The potential role of neutrophils in promoting the metastatic phenotype of tumors releasing interleukin-8. Clin Cancer Res. 2004;10:4895–900.
28. Rosales C. Neutrophil: a cell with many roles in inflammation or several cell types. Front Physiol. 2018;9:113.
29. Charo IF, Ransohoff RM. The many roles of chemokines and chemokine receptors in inflammation. N Engl J Med. 2006;354:610–21.
30. Capucetti A, Albano F, Bonecchi R. Multiple roles for chemokines in neutrophil biology. Front Immunol. 2020;11:1259.
31. Hu N, Westra J, Rutgers A, Doornbos-Van der Meer B, Huitema MG, Stegeman CA, et al. Decreased CXCR1 and CXCR2 expression on neutrophils in anti-neutrophil cytoplasmic autoantibody-associated vasculitides potentially increases neutrophil adhesion and impairs migration. Arthritis Res Ther. 2011;13:R201.
32. Nolan KF, Strong V, Soler D, Fairchild PJ, Cobbold SP, Croxton R, et al. IL-10-conditioned dendritic cells, decommissioned for recruitment of adaptive immunity, elicit innate inflammatory gene products in response to danger signals. J Immunol. 2004;172:2201.
33. Das T, Chen Z, Hendriks RW, Kool M. A20/tumor necrosis factor α-induced protein 3 in immune cells controls development of autoinflammation and autoimmunity: lessons from mouse models. Front Immunol. 2018;9:104.
34. Regan-Komito D, Valaris S, Kapellos TS, Recio C, Taylor L, Greaves DR, et al. Absence of the non-signalling chemerin receptor CCRL2 exacerbates acute inflammatory responses in vivo. Front Immunol. 2017;8:1621.
35. Mandeville I, Aubin J, LeBlanc M, Lalancette-Hébert M, Janelle MF, Tremblay GM, et al. Impact of the loss of Hoxa5 function on lung alveogenesis. Am J Pathol. 2006;169:1312–27.
36. Becker F, Potepalov S, Shehzahdi R, Bernas M, Witte M, Abreo F, et al. Down-regulation of FoxC2 increased susceptibility to experimental colitis: influence of lymphatic drainage function? Inflamm Bowel Dis. 2015;21:1282–96.
37. George T, Bell M, Chakraborty M, Siderovski DP, Giembycz MA, Newton R. Protective roles for RGS2 in a mouse model of house dust mite-induced airway inflammation. PLoS One. 2017;12:e0170269.
38. Immler R, Simon SI, Sperandio M. Calcium signalling and related ion channels in neutrophil recruitment and function. Eur J Clin Invest. 2018;48:e12964.
39. Béguin P, Nagashima K, Mahalakshmi RN, Vigot R, Matsunaga A, Miki T, et al. BARP suppresses voltage-gated calcium channel activity and Ca^{2+}-evoked exocytosis. J Cell Biol. 2014;205:233–49.
40. Liu T, Zhang L, Joo D, Sun SC. NF-κB signaling in inflammation. Signal Transduct Target Ther. 2017;2:17023.
41. Maguire O, O'Loughlin K, Minderman H. Simultaneous assessment of NF-κB/p65 phosphorylation and nuclear localization using imaging flow cytometry. J Immunol Methods. 2015;423:3–11.
42. Martínez-Reyes I, Chandel NS. Mitochondrial TCA cycle metabolites control physiology and disease. Nat Commun. 2020;11:102.
43. Liu Y, Beyer A, Aebersold R. On the dependency of cellular protein levels on mRNA abundance. Cell. 2016;165:535–50.
44. Dewenter M, Pan J, Knödler L, Tzschöckel N, Henrich J, Cordero J, et al. Chronic isoprenaline/phenylephrine vs. exclusive isoprenaline stimulation in mice: critical contribution of alpha(1)-adrenoceptors to early cardiac stress responses. Basic Res Cardiol. 2022;117:15.
45. Butterfield TA, Best TM, Merrick MA. The dual roles of neutrophils and macrophages in inflammation: a critical balance between tissue damage and repair. J Athl Train. 2006;41:457–65.
46. Watanabe S, Alexander M, Misharin AV, Budinger GRS. The role of macrophages in the resolution of inflammation. J Clin Invest. 2019;129:2619–28.
47. Kim Y, Nurakhayev S, Nurkesh A, Zharkinbekov Z, Saparov A. Macrophage polarization in cardiac tissue repair following myocardial infarction. Int J Mol Sci. 2021;22:2715.
48. Tang KM, Wang GR, Lu P, Karas RH, Aronovitz M, Heximer SP, et al. Regulator of G-protein signaling-2 mediates vascular smooth muscle relaxation and blood pressure. Nat Med. 2003;9:1506–12.
49. Schioppa T, Sozio F, Barbazza I, Scutera S, Bosisio D, Sozzani S, et al. Molecular basis for CCRL2 regulation of leukocyte migration. Front Cell Dev Biol. 2020;8:615031.
50. Sjögren B, Parra S, Atkins KB, Karaj B, Neubig RR. Digoxin-mediated upregulation of RGS2 protein protects against cardiac injury. J Pharmacol Exp Ther. 2016;357:311–9.

51. Li HM, Li KY, Xing Y, Tang XX, Yang DM, Dai XM, et al. Phenylephrine attenuated sepsis-induced cardiac inflammation and mitochondrial injury through an effect on the PI3K/Akt signaling pathway. J Cardiovasc Pharmacol. 2019;73:186–94.
52. Li PL, Liu H, Chen GP, Li L, Shi HJ, Nie HY, et al. STEAP3 (six-transmembrane epithelial antigen of prostate 3) inhibits pathological cardiac hypertrophy. Hypertension. 2020;76:1219–30.
53. Kumar S, Wang G, Liu W, Ding W, Dong M, Zheng N, et al. Hypoxia-induced mitogenic factor promotes cardiac hypertrophy via calcium-dependent and hypoxia-inducible factor-1α mechanisms. Hypertension. 2018;72: 331–42.
54. Yamamura S, Izumiya Y, Araki S, Nakamura T, Kimura Y, Hanatani S, et al. Cardiomyocyte Sirt (Sirtuin) 7 ameliorates stress-induced cardiac hypertrophy by interacting with and deacetylating GATA4. Hypertension. 2020;75: 98–108.
55. Soehnlein O, Lindbom L, Weber C. Mechanisms underlying neutrophil-mediated monocyte recruitment. Blood. 2009;114:4613–23.
56. Silvestre-Roig C, Braster Q, Ortega-Gomez A, Soehnlein O. Neutrophils as regulators of cardiovascular inflammation. Nat Rev Cardiol. 2020;17:327–40.
57. Schiattarella GG, Rodolico D, Hill JA. Metabolic inflammation in heart failure with preserved ejection fraction. Cardiovasc Res. 2021;117:423–34.
58. Tannahill GM, Curtis AM, Adamik J, Palsson-McDermott EM, McGettrick AF, Goel G, et al. Succinate is an inflammatory signal that induces IL-1β through HIF-1α. Nature. 2013;496:238–42.
59. Wong HS, Dighe PA, Mezera V, Monternier PA, Brand MD. Production of superoxide and hydrogen peroxide from specific mitochondrial sites under different bioenergetic conditions. J Biol Chem. 2017;292:16804–9.
60. Amin JK, Xiao L, Pimental DR, Pagano PJ, Singh K, Sawyer DB, et al. Reactive oxygen species mediate alpha-adrenergic receptor-stimulated hypertrophy in adult rat ventricular myocytes. J Mol Cell Cardiol. 2001;33:131–9.
61. Xiao L, Pimentel DR, Wang J, Singh K, Colucci WS, Sawyer DB. Role of reactive oxygen species and NAD(P)H oxidase in alpha(1)-adrenoceptor signaling in adult rat cardiac myocytes. Am J Physiol Cell Physiol. 2002;282:C926–34.
62. Mittal M, Siddiqui MR, Tran K, Reddy SP, Malik AB. Reactive oxygen species in inflammation and tissue injury. Antioxid Redox Signal. 2014;20:1126–67.
63. Zhou B, Tian R. Mitochondrial dysfunction in pathophysiology of heart failure. J Clin Invest. 2018;128:3716–26.
64. Strassheim D, Dempsey EC, Gerasimovskaya E, Stenmark K, Karoor V. Role of inflammatory cell subtypes in heart failure. J Immunol Res. 2019;2019:2164017.
65. Redfors B, Vedad R, Angerås O, Råmunddal T, Petursson P, Haraldsson I, et al. Mortality in takotsubo syndrome is similar to mortality in myocardial infarction—a report from the SWEDEHEART registry. Int J Cardiol. 2015;185:282–9.
66. Isogai T, Matsui H, Tanaka H, Fushimi K, Yasunaga H. Early β-blocker use and in-hospital mortality in patients with Takotsubo cardiomyopathy. Heart. 2016;102:1029–35.
67. Perez-Riverol Y, Bai J, Bandla C, García-Seisdedos D, Hewapathirana S, Kamatchinathan S, et al. The PRIDE database resources in 2022: a hub for mass spectrometry-based proteomics evidence. Nucleic Acids Res. 2022;50:D543–d52.